Synthesis and Textural Characterization of Mesoporous and Meso-/Macroporous Silica Monoliths Obtained by Spinodal Decomposition

Anne Galarneau, Zakaria Abid, Bilel Said, Youcef Did, Katarzyna Szymanska, Andrzej Jarzebski, Franck Tancret, Hadj Hamaizi, Abdelkader Bengueddach, Francesco Di Renzo, et al.

inorganics

MDPI

Article

Synthesis and Textural Characterization of Mesoporous and Meso-/Macroporous Silica Monoliths Obtained by Spinodal Decomposition

Anne Galarneau [1,*], Zakaria Abid [1,2], Bilel Said [1], Youcef Didi [1], Katarzyna Szymanska [3], Andrzej Jarzębski [3,4], Franck Tancret [5], Hadj Hamaizi [2], Abdelkader Bengueddach [2], Francesco Di Renzo [1] and Francois Fajula [1]

1 Institut Charles Gerhardt Montpellier, UMR 5253 CNRS-Université de Montpellier-ENSCM, ENSCM, 8 rue de l'Ecole Normale, 34296 Montpellier Cedex 05, France; zakariabid@yahoo.fr (Z.A.); bilel.said@enscm.fr (B.S.); youcef.didi@enscm.fr (Y.D.); francesco.di-renzo@enscm.fr (F.D.R.); ffajula@enscm.fr (F.F.)

2 Laboratoire de Chimie des Matériaux, Faculté des Sciences Appliquées et Exactes, University of Oran 1 Ahmed Ben Bella, BP 1524 Oran, Algeria; hamaizimizou@yahoo.fr (H.H.); abengueddach@gmail.com (A.B.)

3 Department of Chemical Engineering and Process Design, Silesian University of Technology, 44-100 Gliwice, Ks. M. Strzody 7, Poland; Katarzyna.Szymanska@polsl.pl (K.S.); Andrzej.Jarzebski@polsl.pl (A.J.)

4 Institute of Chemical Engineering, Polish Academy of Sciences, 44-100 Gliwice, Bałtycka 5, Poland

5 Université de Nantes, Institut des Matériaux de Nantes-Jean Rouxel (IMN), Polytech Nantes, Rue Christian Pauc, BP 50609, 44306 Nantes Cedex 3, France; Franck.Tancret@univ-nantes.fr

* Correspondence: anne.galarneau@enscm.fr; Tel.: +33-4-6716-3468

Academic Editors: Samuel Bernard, Andre Ayral and Philippe Miele
Received: 26 February 2016; Accepted: 22 March 2016; Published: 18 April 2016

Abstract: Silica monoliths featuring either mesopores or flow-through macropores and mesopores in their skeleton are prepared by combining spinodal phase separation and sol-gel condensation. The macroporous network is first generated by phase separation in acidic medium in the presence of polyethyleneoxides while mesoporosity is engineered in a second step in alkaline medium, possibly in the presence of alkylammonium cations as surfactants. The mesoporous monoliths, also referred as aerogels, are obtained in the presence of alkylpolyethylene oxides in acidic medium without the use of supercritical drying. The impact of the experimental conditions on pore architecture of the monoliths regarding the shape, the ordering, the size and the connectivity of the mesopores is comprehensively discussed based on a critical appraisal of the different models used for textural analysis.

Keywords: silica monolith; aerogel; pressure drop; pore size; pore shape; hierarchical material

1. Introduction

Porous silica monoliths with controlled pore sizes and high surface area are of particular interest for process intensification of numerous continuous flow applications in catalysis, adsorption or separation [1] and for applications requiring self-standing bodies [2,3] featuring adjustable and controlled pore sizes such as Li-ion batteries [4] or super thermal insulators [5,6]. Mesoporous silica monoliths (containing or not macropores) are also of great interest as porous model materials to investigate transport phenomena of ions or molecules avoiding any shaping of powders by compacting. Silica monoliths obtained by spinodal decompostition exhibit homogeneous interconnected pore networks at the mesopore and/or the macropore scale. Spinodal decomposition therefore constitutes a unique tool for producing ordered bicontinuous homogeneous porous structures that significantly enhance mass transport. Porous silica monoliths can be obtained by either physical or chemical spinodal decompositions.

Physical spinodal decomposition is used for decades to produce porous glasses, well known under the names of CPG or Vycor [7]. Porous glasses are formed by mixing at high temperature (1200 °C) two solids as SiO_2 and B_2O_3 in the presence of alkaline oxides M_2O (with M = Na, K or Li) to obtain a single thermodynamic alloy alkali borosilicate phase, which is then rapidly cooled to a temperature at which thermodynamic equilibrium favors a silica-rich phase coexisting with a borate-rich phase. Spinodal decomposition occurs when silica species and borates species begin to cluster together into silica-rich and borate-rich clusters by diffusion. These clusters then rapidly grow and coalesce to yield a single silica-rich cluster, the silica-rich phase, and a single borate-rich cluster, the borate-rich phase. In effect, a monolith of these two coexisting homogeneous continuous phases is formed, then the borate-rich phase is removed by chemical leaching by mineral acids, water or alcohols at 100 °C leading to a porous silica with a homogeneous interconnected pore network in the mesoporous range from 2 to 1000 nm depending on the synthesis conditions. Interestingly, various geometric shapes of porous glasses can be obtained. The porous glasses obtained by physical spinodal decomposition feature surface areas of 100–300 m^2/g. Attempts made to increase the surface area by pseudomorphic transformation of the porous glasses into MCM-41 allowed a high surface area of 1000 m^2/g for a mesopore diameter of 3.7 nm [7]. However to obtain high surface area silica monoliths (600–1200 m^2/g), chemical spinodal decomposition is preferred. The synthesis procedure is direct and does not need high temperature (above 1000 °C) treatment, affording a less energetic demanding process and a better control of porosity.

Chemical spinodal decomposition is a mechanism for the rapid unmixing of a homogeneous mixture of hydrated silica species/polymer/water from a single phase to form two coexisting phases. Typically, the homogeneous mixture of silica species/polymer and water is maintained into a single thermodynamic phase at low temperature (0–20 °C) in which silica species are surrounded by water and polymer molecules. Then the mixture is heated up at temperature above *ca.* 40 °C, silica species start condensate into silica oligomers or clusters and polymers start interacting with the newly formed silica surface. This is the starting point of the spinodal decomposition leading to phase separation into a silica/polymer-rich phase and a water-rich phase. The chemical spinodal decomposition is a kinetic process, where the two phases grow within time and the final state is obtained when the silica oligomers are condensed, at the sol-gel transition of silica. The size and topology of the silica-rich phase will determine the size and topology of the monolith skeleton and the size and topology of the water-rich phase the size and topology of the pore network. The pore size is controlled by the rate of the silica condensation, which in turn is controlled by the temperature, the amount of acid, the amount and type of polymer [8–12].

In this study, silica mesoporous or hierarchical mesoporous/macroporous monoliths have been obtained by chemical spinodal decomposition in acidic medium using polyethylene (PEO) based polymers. We will detail the synthesis procedures enabling to control the pore sizes, their homogeneity and critically characterize the pore architecture. The relevance of macropore and mesopore architecture networks in controlling pressure drop and mass transfer, respectively, in continuous flow applications will be highlighted.

2. Results and Discussion

2.1. Silica Monoliths with Hierarchical Macro- and Mesoporosity

2.1.1. Control of Macroporosity

Silica monoliths of 6 mm diameter and 10 cm length exhibiting a hierarchical network of macro- and mesopores have been synthesized by chemical spinodal decomposition using polyethylene oxides (PEO) of 10 to 100 kDa in acidic (HNO_3) aqueous medium in the presence of tetraethylorthosilicate as silica source. The mathematical theory of spinodal decomposition is based largely on the development of a generalized diffusion equation [13,14]. The mechanism of spinodal decomposition can be visualized via an animation [15], illustrating the microstructural evolution under the Cahn–Hilliard

equation, showing distinctive coarsening and phase separation (Figure 1). The phase separation ends at the sol-gel transition. The macropore size will be determined by the sol-gel transition kinetics and controlled by the size of the polymer, the ratio of EO unit/Si and the amount of acid. For a constant composition of the mixture (1 Si:14.21 H_2O:0.60 EO unit:0.26 HNO_3) increasing the size of the polymer increases the size of the macropore and in the same time of the skeleton thickness. For PEO of 20, 35, and 100 kDa, macropore sizes of 4, 10, and 16 microns and skeleton thickness of 3, 6, and 7 microns have been obtained, respectively [9]. Lower molecular weight PEO polymers interact more strongly with silica oligomers via multiple interactions, they adsorb at the surface of the silica oligomer and cover the particle, leading to a faster condensation of the silica oligomers and favor the sol-gel transition, resulting in smaller pores. Higher molecular weight PEO polymers form loops on the silica surface, leading to an increase of the thickness of the adsorbed layer [16] inducing a slower rate of condensation of silica oligomers and therefore slow down the sol-gel transition. For a given size of polymer as PEO 20 kDa, increasing the amount of polymer decreases the size of the macropores. For a composition mixture 1 Si:14.21 H_2O:x EO unit:0.26 HNO_3 with x = 0.55, 0.60, 0.65, macropore size of 8, 4, 1 microns and skeleton thickness of 5, 3, 1 microns have been obtained, respectively (Figure 2). Increasing the amount of polymer favors silica oligomer aggregation and therefor favors the sol-gel transition. However the monolith obtained for EO unit/Si = 0.65 is fragile due maybe to a lower condensation state of silica with to high interactions between EO unit and silica. In the monolith obtained for EO unit/Si = 0.55, the skeleton of the monolith features additional macropores presumably due to a second phase separation inside the skeleton. The same control of macropore size with increasing amount of EO unit/Si was previously observed for PEO 10 kDa. For a composition mixture 1 Si:~14.5 H_2O:x EO unit:0.26 HNO_3 where x = 0.52, 0.59, and 0.63, macropore size of 20, 10 and 4 microns were obtained, respectively [17]. These authors showed also that increasing the amount of acid decreases the size of the macropores. For a composition mixture 1 Si:~15 H_2O:0.63 EO unit:x HNO_3 where x = 0.26 and 0.41, macropore sizes of 4 and 1 microns were obtained, respectively [17]. Increasing the amount of acid will accelerate the sol-gel transition.

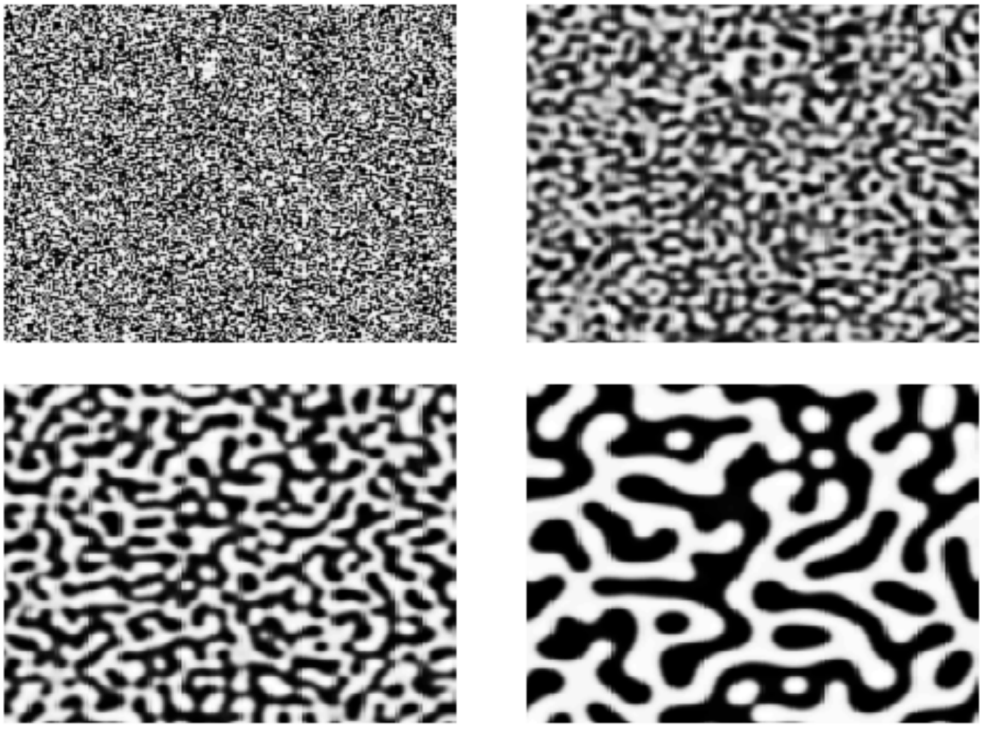

Figure 1. Schematic evolution of spinodal decomposition during time, adapted from [15].

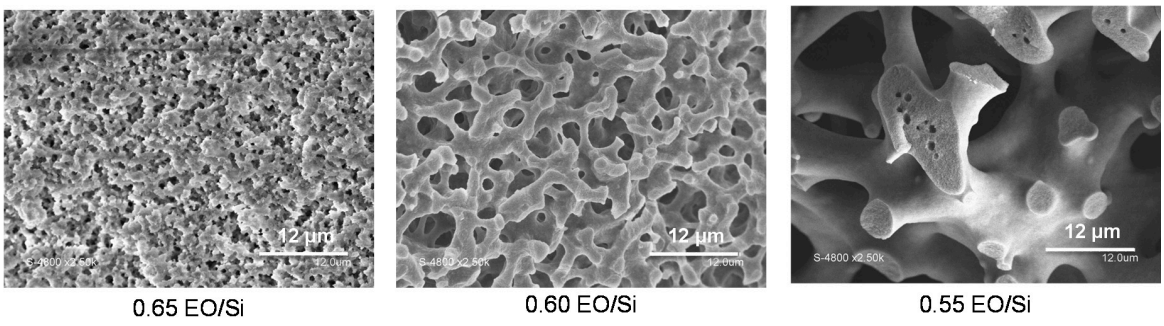

Figure 2. SEM images of the macrostructures of hierarchical silica monoliths as a function of ethylene oxide (EO) unit/Si molar ratio in the synthesis.

2.1.2. Control of Pressure Drop for Liquid Flow Processes

The control of macropore size and its homogeneity is of paramount importance for liquid flow processes such as separation, catalysis, adsorption, ion-exchange, wastewater treatment, *etc.* Except in liquid chromatography (where high pressure instruments are used), most applications require materials generating low pressure drops (<1 bar/cm) under flow operation. Establishing relationships between pressure drop and macropore size for materials with macropores shape different from cylindrical shape has barely been attempted and is of prime importance to predict pressure drop in an application. This was done for the first time here in the case of the complex macroporous structure of silica monoliths prepared by phase separation. It has been shown that silica monoliths with hierarchical porosity (macro-/mesoporous) prepared by chemical spinodal decomposition develop laminar flow due to the homogeneous macropore network with, a pressure drop linearly proportional to the flow rate [17] (Figure 3). Upon increasing the flow rate, the pressure drop increases dramatically when the size of the macropore decreases (Figure 3a). Flows through porous media in macroscale have to satisfy empirical Darcy's law [18]. Considering a porous medium as a system consisting of straight tubes of diameter d and length l, the elementary pressure drop can be described using the well-known Darcy–Weissbach equation:

$$\frac{\Delta P}{l} = \lambda \frac{w^2 \rho}{2d} \tag{1}$$

Due to small liquid velocities in the monolith the friction drag coefficient λ can be calculated from the formula developed for laminar flow using the Reynolds number Re:

$$\lambda = \frac{a}{\mathrm{Re}} \tag{2}$$

where a is so-called geometrical coefficient and depends on the shape of the flow channel. To eliminate liquid velocity w from Equation (1), liquid flow rate $\dot{V}$ (mL/min) can be used together with cross section area A of the monolith and its volume porosity ε. Using definition formula for Re number (Re = ρdw/η) and the viscosity of the fluid η, the pressure drop equation becomes:

$$\frac{\Delta P}{l} = \frac{a}{2\varepsilon d^2} \frac{\eta}{A} \dot{V} \tag{3}$$

Average pores length l and monolith unit length L are not the same due to some stochastic direction changes called tortuosity τ, defined as:

$$\tau = \frac{l}{L} \tag{4}$$

Putting Equation (4) in Equation (3), the pressure drop at given monolith unit length can be expressed as follows:

$$\frac{\Delta P}{L} = \frac{a\tau}{2\varepsilon d^2}\frac{\eta}{A}\dot{V} \quad (5)$$

Although average value of the two geometrical parameters, porosity ε and macropore diameter d, could be measured by mercury porosimetry, tortuosity τ cannot be separated from the channel shape a coefficient. Thus for practical reasons, all of these parameters of Equation (5) can be combined in one called Darcy permeability coefficient K, and the drop pressure equation can be expressed as followed:

$$\frac{\Delta P}{L} = \frac{1}{K}\frac{\eta}{A}\dot{V} \quad (6)$$

where

$$K = \frac{2\varepsilon}{a\tau}d^2 \quad (7)$$

Darcy permeability coefficient K given in Equations (6) and (7) enables the comparison of porous materials for a given fluid and its value is relatively easy to determine by plotting pressure drop divided by the length of the monolith as a function of lineic flow, which is the flow (mL/min) divided by the cross section of the monolith (0.28 cm^2 in our case) (Figure 3b). Macropore sizes of four monoliths prepared by chemical spinodal decomposition have been determined by mercury porosimetry, which gave a distribution of macropore diameter for each monolith: (1) 1–2 µm; (2) 3–6 µm; (3) 10–15 µm; and (4) 20–30 µm. By using water as a model liquid (viscosity: 1.002 mPa· s at 20 °C) under different flow rates, the resulting Darcy permeability coefficient K were calculated from the slopes of the plots of pressure drop *vs.* flow rate (Figure 3b) and were found equal to 0.21, 0.84, 5.57, and 19.6 μm^2, respectively.

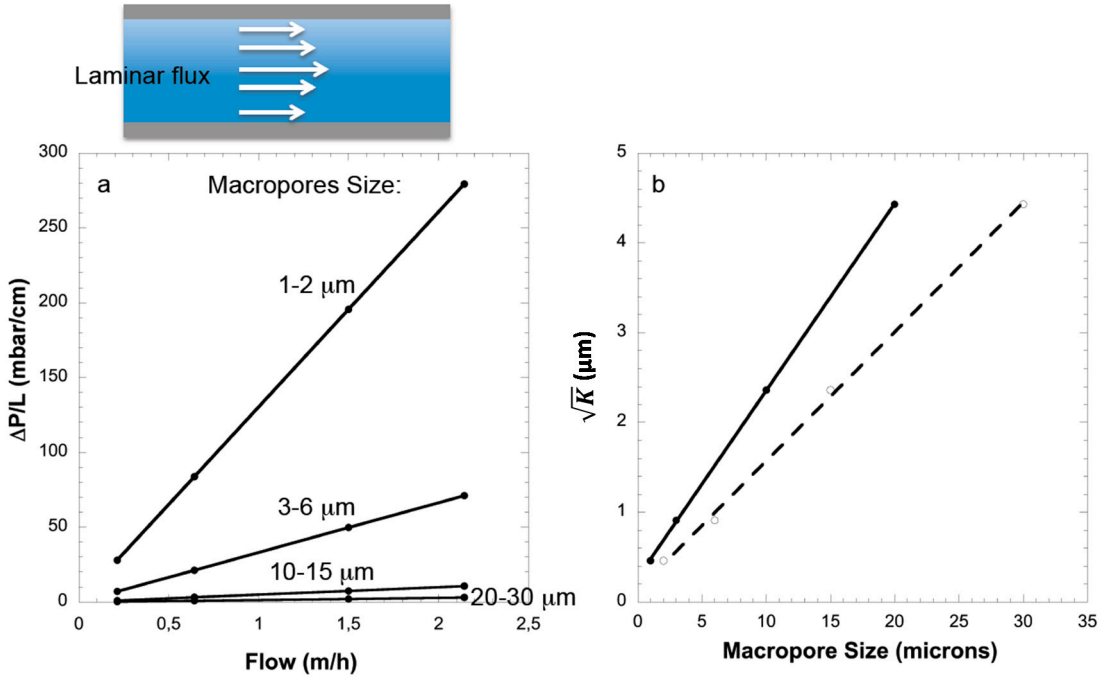

Figure 3. (**a**) Pressure drop as a function of linear velocity and macropore diameter of hierarchical silica monoliths; (**b**) square root of permeability (K) of the hierarchical silica monoliths as a function of macropore diameter (minimum diameter (plain line), maximum diameter (dashed line)).

The Darcy permeabilities can be expressed in Darcy (D or μm^2) and are characterized as follows:

Zero and low permeability: $<10^{-6}$ μm^2
Average permeability: 0.015–0.050 μm^2
Good permeability: 0.050–0.250 μm^2
Very good permeability: 0.250–1 μm^2
Excellent permeability: >1 μm^2

Therefore the permeability of the silica monoliths is good for macropores size of 1–2 μm, very good for macropores size of 3–6 μm and excellent for macropores size above 10 μm. These monoliths could be used as model materials of porous rocks as their permeability is comparable to sandstone (permeability in the range of 1 Darcy). The permeability depends on numerous features of porosity: pore volume, pore size, pore shape and pore connectivity. In the case of model of parallel cylindrical channels, the permeability can be expressed as:

$$K = \frac{\varepsilon}{2}\left(\frac{d}{4}\right)^2$$

where ε the porosity equal to the ratio of pore volume and total volume. In the case of monoliths, the shape of the pores is difficult to describe numerically. However, by plotting the square root of K as a function of macropore diameters (with either the minimum or the maximum limit of macropore size), linear relationships have been found:

for the minimum size of macropore:

$$\sqrt{K} = \frac{1}{4.80}d + \frac{1}{3.71} \approx \frac{1}{4}(d+1)$$

for the maximum size of macropore:

$$\sqrt{K} = \frac{1}{6.97}d + \frac{1}{7.46} \approx \frac{1}{7}(d+1)$$

Note that the permeability K is not zero for a monolith with no macroporosity. This could be explained by small space between the resin clad and the monolith of *ca.* 0.5 μm around the monolith.

Using these equations, it is possible to predict the permeability and the pressure drop for monoliths obtained by chemical spinodal decomposition just by knowing their macropore size. The porosity of the silica monoliths is $0.7 < \varepsilon < 0.8$ if only macropores are taken into account and above $\varepsilon > 0.9$ if mesopore and macropore volumes are considered. As a first approximation, one can use the following simple empirical formula to estimate the permeability of a monolith prepared by chemical spinodal decomposition:

$$\left(\frac{d}{7}\right)^2 \leqslant K \leqslant \left(\frac{d}{4}\right)^2$$

Considering that the smallest macropore size determined by mercury intrusion strongly affect the pressure drop, in first approximation: $K = (d/4)^2$. This value is very close to $K = (1/2)(d/4)^2$ with $\varepsilon \sim 1$ which is the permeability coefficient for the laminar flow into cylindrical tubes. This means that permeability of silica monoliths prepared by chemical spinodal decomposition, despite their complex macropores network geometry, tends to that of a bunch of cylindrical tubes and that can be attributed to the extensive connectivity of the macropores network.

For catalysis, it has been shown that a ratio of monolith length to monolith diameter of at least 5 is recommended [19]. Therefore, for 6 mm diameter silica monolith, a minimum length of 3 cm is needed. For applications demanding linear velocities (flow rate divided by monolith cross section) higher than

1 m/h (at least 0.5 mL/min for silica monolith of 6 mm of diameter), all monoliths can be used with a pressure drop lower than 1 bar. For applications requiring a very low pressure drop (<10 mbars), only the monoliths with 20 microns macropores could be used. However, skeleton thickness increases as the same time of macropore size, whereas only thinner skeleton struts enable good internal mass transfer in the mesopores [1]. Therefore, for macro-/mesoporous monoliths, there is a compromise to find between low pressure drop and high internal mass transfer in the mesoporosity. For many applications, as in catalysis, adsorption or ionic-exchange, we have chosen monoliths featuring macropores of 4 microns and a skeleton thickness of 3 microns to satisfy this compromise [1].

2.1.3. Influence of Mesopores Shape and Connectivity in Diffusion

The mass transfer in the mesoporosity of materials can be calculated by the Van Deemter equation. A high mass transfer is reached for a low C parameter of the Van Deemter equation, which is proportional to the square of the diffusion length (particle diameter for a packed-bed or the skeleton thickness for the monolith) [1,20]. We have shown previously that mass transfer in the mesoporosity is also controlled by the size of the mesopores (or more exactly the ratio mesopore diameter/molecule diameter), the homogeneity of the mesopore size distribution (cylindrical pores and pores with constrictions assimilated to spherical pores) and the interconnectivity of the mesopore network [1,20]. The C parameter of the Van Deemter equation is inversely proportional to the diffusion D_{iff} into the pore:

$$C = \frac{C_{sm}}{D_{iff}} d_P^2$$

where d_p the particle diameter or skeleton thickness and C_{sm} a constant for a given molecule in relation with the affinity of the molecule to the pore.

Therefore, the diffusion inside mesopores is proportional to 1/C. Using spherical silica particles of 10 microns and for a given molecule (diethylphtalate), we have shown that diffusion in mesopores increases with the pore diameter, with the presence of interconnections in the mesoporous network and decreases for mesopores featuring constrictions assimilated to spherical cavities. This analysis was done thanks to materials prepared by the pseudomorphic transformation of spherical silica particles (named LiChrospher 60) featuring interconnected spherical pores (cavity 6.8 nm) into either MCM-41 type mesoporosity (cylindrical non-connected pores of 3.7 nm), MCM-48 type mesoporosity (cylindrical interconnected pores of 3.4 nm), MCM-41 swelled with TMB (cylindrical pores of 6.8 nm), or MCM-41 swelled with TMB/decane mixture (unconnected spherical pores with cavities 6.8 nm). It has been shown that diffusion was directly proportional to mesopore sizes (mesopore diameter for cylindrical pores and mesopore cavity for spherical pores) and that a correction m has to be added for the shape of the pore (m = 2 for cylindrical pores, m = 3 for spherical pores) [21].

By plotting 1/C as a function of pore size (diameter or cavity) we can have an indication of the evolution of the diffusion (as 1/C is proportional to it) and we have determined linear relationships between 1/C (or diffusion) and pore diameters (Figure 4). The slopes of the lines show the evolution of the diffusion rate as a function of pore size, shape and connectivity. Slopes of 0.0128, 0.0088, 0.0082, and 0.0056 $ms^{-1} \cdot nm^{-1}$ were obtained for cylindrical interconnected pores, cylindrical non-connected pores, spherical interconnected pores, and unconnected spherical pores with cavities, respectively. A general empirical relationship between diffusion, pore size and shape can be proposed by examining these results as:

$$D_{iff} = \frac{C_{sm}}{C} d_P^2 = \mathrm{A}\left(\frac{1}{C}\right) = \mathrm{B}\left(\frac{t}{m}\right)\left(\frac{D}{\sigma}\right)$$

where A and B are constants, D is the pore diameter or the cavity size, σ is the molecule diameter, m is the geometrical factor (m = 2 for cylindrical pore, m =3 for spherical pore), and t is the connections factor (t = 1 for no connections between pores, t = 1.45 for connections between pores).

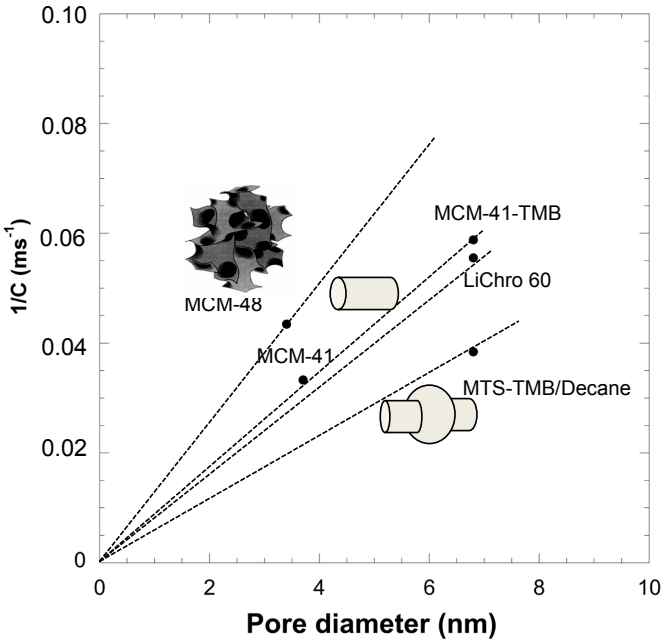

Figure 4. Inverse of C parameter of Van Deemter equation (1/C) as a function of mesopore size (diameter for cylindrical pores, cavity size for spherical pores) for different mesoporous silica materials of 10 microns particles size. C values calculated for diethylphtalate in dioxane/heptane mobile phase [20].

For a given pore size, the highest diffusion in mesopores follows the sequence: interconnected cylindrical pores > cylindrical pores ~ interconnected spherical pores > spherical pores. From the discussion above, it appears that it is not only very important to control the size of the mesopores, but also their shape and connectivity in the mesoporous network in order to control the diffusion and, as a consequence, the contact time of any process. Regarding reactivity in catalytic reactions, we have also shown that a compromise should be reached between mesopore size and availability of active surface for the reaction. An optimal mesopore diameter corresponding to around 5–7 times the reactant molecule diameter was found by applying the Ruckenstein rule [1,22]. This value corresponds to a same amount of molecules able to adsorb on the surface of the pores and able to diffuse inside the volume of the pore.

2.1.4. Characterization of the Mesoporosity in Hierarchical Silica Monoliths: Pore Size, Pore Shape, Ordering and Connectivity

To understand and control diffusion in silica monoliths, it is important to characterize precisely their mesoporous volume, surface area, mesopore diameter, shape and connectivity. Silica monoliths with hierarchical porosity (meso-/macroporous) have been prepared by a two steps process. The first step is performed in acidic medium where the spinodal decomposition occurs followed by the sol-gel transition to stop the phase separation to form the macroporosity and in the second step the monolith is placed in a basic medium (NH_4OH) to generate mesopores by an Ostwald ripening mechanism. The silica network formed in acidic medium is weakly condensed and in basic medium the silica network rearranges into silica nanoparticles, which creates mesopores in the interparticles space. The mesopores diameters depend on the basic temperature and treatment duration.

At a constant reaction temperature of 40 °C in NH_4OH, the mesopore diameter increases from 2 to 12 nm for duration of 1 to 24 h with a constant surface area of 700 m^2/g with concomitant increase of pore volume from 0.4 to 1.1 mL/g (Figure 5). Crack-free monoliths are obtained for treatments

durations above 6 h at 40 °C. From the specific surface area S, we can calculate the average diameter d of the nanoparticles inside the monolithic skeleton from the formula:

$$d = 6/S\rho$$

with ρ being the silica density (2.2 g/cm^3)

For S = 700 m^2/g, the silica nanoparticles diameter is 4 nm. The increase of the mesopore diameter is due to a reorganization of these nanoparticles into larger structures upon basic treatment as shown in Figure 5. Increasing the basic treatment duration above 24 h will not increase the pore diameter. It seems that the more stable nanoparticles organization is reached when a void equal to ~3 times the size of the nanoparticles is formed. To further increase the mesopore diameter, the temperature of the basic treatment has to be raised. By maintaining the basic treatment duration for 24 h and increasing the temperature from 40 to 80 °C, the mesopore diameters increase from 12 to 25 nm, the pore volumes increase from 1.1 to 1.3 mL/g with a concomitant surface areas decrease from 700 to 400 m^2/g. This corresponds to the increase of silica nanoparticles size from 4 to 9 nm inside the skeleton of the monolith due to Ostwald ripening, but the organization of the nanoparticles remains similar (Figure 5).

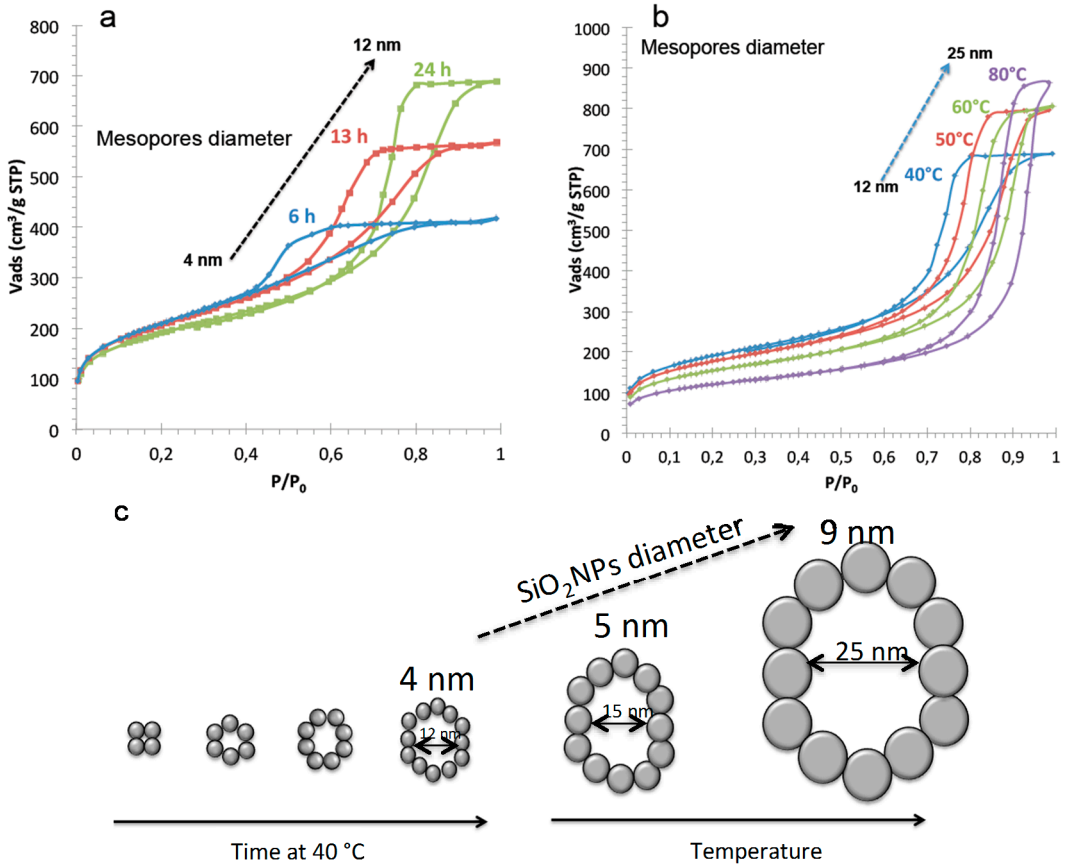

Figure 5. Nitrogen sorption isotherms at 77 K of hierarchical silica monoliths prepared with basic (NH_4OH) treatment (**a**) at 40 °C for different time; (**b**) for 24 h at different temperature; and (**c**) Schematic representation of the evolution (size and organization) of the silica nanoparticles inside the skeleton of the monolith during basic treatment.

To determine the shape of the mesopores, geometrical pore diameters calculations were performed with the ratio of pore volumes to pore surfaces using the formula:

$D = 4V/S$ for cylindrical pores
$D = 6V/S$ for spherical pores

It is to recall that specific surface areas S are obtained from the nitrogen isotherm using the BET equation (see below) in which the value of the surface area of the nitrogen molecule is taken as 0.162 nm^2 by default.

$$\frac{p/p_0}{V\,(1-p/p_0)} = \frac{1}{V_m C_{BET}} + \frac{C_{BET}-1}{V_m C_{BET}}\,(p/p_0)$$

To accurately find the linear domain of the BET equation, the use of the Rouquerol criterion [23] should be applied. This is done by plotting $V(1-p/p_0) = f(p/p_0)$ and the first maximum of the curve gives the higher pressure (p/p_0) to use in the BET linear domain. Classically, it is admitted that the BET equation is linear in the domain $0.05 < p/p_0 < 0.35$, but for silica materials, the linear domain is mostly $0.1 < p/p_0 < 0.25$.

By plotting the BET equation, one can calculate V_m, the nitrogen monolayer volume, and C_{BET} parameter from the slope a and the intercept b of the plot:

$$C_{BET} = \frac{a}{b} + 1 \text{ and } V_m = \frac{1}{a+b}$$

$$S_{BET} = \sigma_{N_2} n = \sigma_{N_2} \frac{V_m}{V_{N_2}} N_A$$

where σ_{N_2} is the surface area of the nitrogen molecule at the surface of the material, n is the number of nitrogen molecules, V_{N_2} is the molar volume of nitrogen (22.414 L/mol), and N_A is the Avogadro number (6.025×10^{23} molecule/moles). As V_m is expressed as gas volume in mL STP/g, the surface area becomes:

$$S_{BET}(m^2/g) = 6.025 \sigma_{N_2} V_m$$

and for σ_{N_2} = 0.162 nm^2, S_{BET} (m^2/g) = 4.36 V_m

However, it has been shown that the surface area of a nitrogen molecule is not constant, it changes in function of its interaction with the material surface, as the nitrogen molecule is not spherical but cylindrical [13]. For weak surface interactions, as for nitrogen on organic grafted material or hydrophobic materials, the nitrogen molecules lay on the surface, leading to a surface area projection of 0.162 nm^2, whereas the molecule is more perpendicular to the surface on hydrophilic materials due to stronger affinity and therefore a closer packing, leading to a surface projection close to 0.135 nm^2 (Figure 6). The affinity of nitrogen with the surface can be evaluated by the energy of first layer adsorption of nitrogen molecules on the material surface, which is included in the calculation of the C_{BET} parameter from the BET equation [24].

$$C_{BET} = \alpha \exp\left[(E_1 - E_L)/RT\right]$$

where α is a constant ($\alpha > 0$), E_1 is the energy of adsorption of nitrogen on the surface (first layer) and E_L is the energy of adsorption of the other nitrogen layers assimilated to nitrogen liquefaction energy [24]. C_{BET} is characteristic of adsorbate/material interactions and increases when interactions strength increases. For instance, nitrogen molecules interact strongly with hydrophilic surfaces corresponding to $C_{BET} \sim 100$, whereas for hydrophobic surfaces (as octyl-grafted silicas) [25,26] the interactions are weaker ($C_{BET} \sim 20$) and the projection of the surface area of a nitrogen molecule change from 0.135 to 0.162 nm^2, respectively. For 20–30 < C_{BET} < 90–100, corresponding to hydrophobic–hydrophilic surfaces, the surface of a nitrogen molecules will be $0.135 < \sigma_{N_2} < 0.162$ nm^2. Some corrections of BET surface areas are therefore needed to evaluate the surface area of hydrophilic materials such as silicas. Classical silica materials, as silica monoliths, with silanols on their surface, are hydrophilic ($C_{BET} > 90$),

so corrections of specific BET surface area S_{BET} coming from the instrument are needed and the surface area become S^* using the following formula:

$$S^* = S_{BET} \times (0.135/0.162)$$

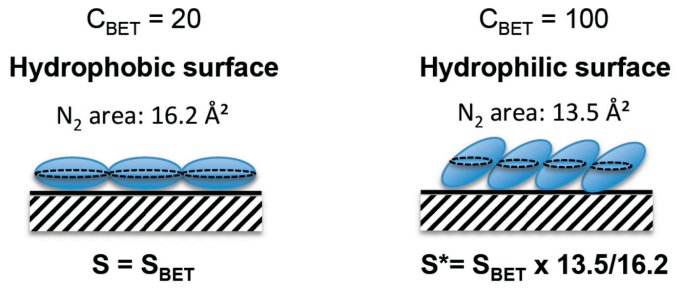

Figure 6. Schematic representation of nitrogen molecules adsorbed at the surface of hydrophobic and hydrophilic materials and the corresponding calculations of specific surface areas.

The geometrical mesopore diameter becomes therefore either equal to $4V/S^*$ for cylindrical pores or to $6V/S^*$ for spherical pores. Pore volumes are taken at the end of the capillary condensation step (Figure 7). For silica monoliths, geometrical pores determination have been compared with mesopore diameters calculated from the capillary condensation pressure using the Broekhoff and De Boer method [27], which proved to be the most accurate method derived from Kelvin equation for mesopore diameter determination. Broekhoff and De Boer method has been proposed for cylindrical pores. However, mesopore size determination is impacted by the shape of the pore and is different for cylindrical and spherical pores. For cylindrical pores, the mesopore diameter is calculated by using the desorption branch of the isotherm and BdB desorption is applied to the mean pressure of desorption. For spherical pores, the constriction diameter of the pore is calculated from the pressure of the closing point of the hysteresis by applying the BdB desorption and the cavity size is calculated from the adsorption branch of the isotherm by applying the BdB desorption to the mean pressure of adsorption (Figure 7). This observation has been confirmed by simulation experiments on various shapes of pores [28–30].

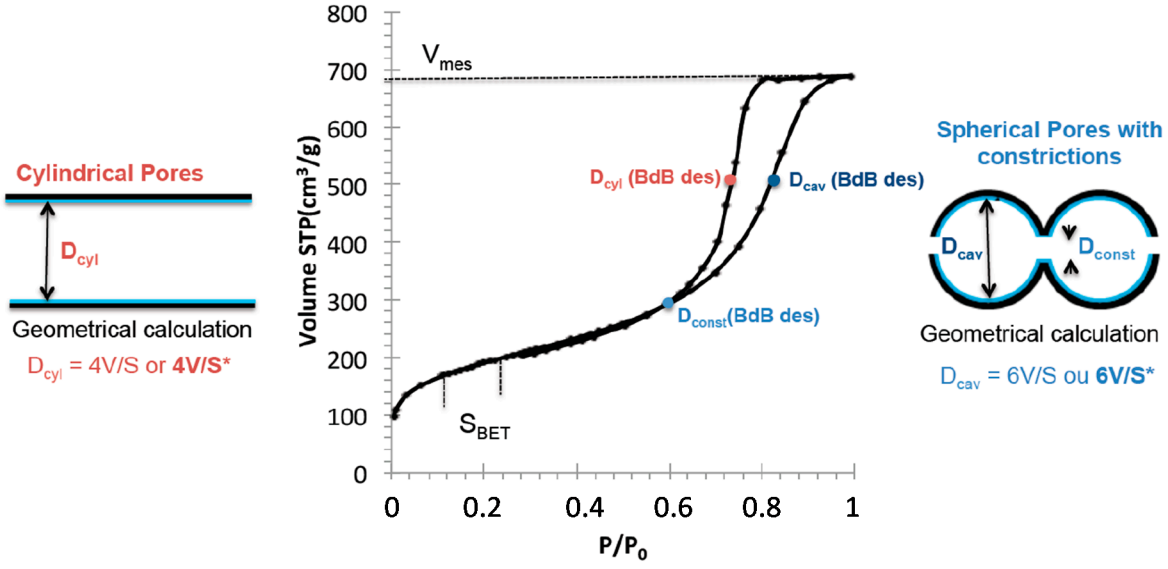

Figure 7. Schematic representation to explain how to measure mesopore size in the case of cylindrical and spherical shape of mesopores.

The use of BdB desorption to the adsorption branch in the case of spherical pores can be explained with the Kelvin equation for cylindrical and spherical pores. Indeed, the Kelvin equation is expressed as:

$$r_k = \frac{-2\gamma V_L}{RT\ln(p/p_0)}$$

with

$$\frac{2}{r_k} = \frac{1}{r_1} + \frac{1}{r_2}$$

where γ is the surface tension of nitrogen at the solid surface, V_L is the molar volume, and r_k describes the curvature of the adsorbate layer at the surface of the pore in two directions: along the pore r_1 and perpendicular to the pore r_2.

For a cylindrical pore, during the desorption, the curvature meniscus is spherical and $r_1 = r_2 = r$, r being the pore radius of the pore and therefore $r_{\text{kdes(cylinder)}} = r$. For spherical pores, during adsorption, the adsorbed layer is spherical and $r_1 = r_2 = r$ with r the radius of the cavity and therefore $r_{\text{kads(sphere)}} = r$. Therefore the Kelvin equation is the same for the adsorption in spherical pores with cavity of radius r and for the desorption in cylindrical pores of radius r. It is precise that the radius r_k determined by the Kelvin equation is not directly the pore diameter r_p as it is only calculated from pore filling. To obtain the pore diameter, the thickness t of the adsorbed layer before capillary condensation has to be added (BJH method):

$$r_{\text{p}} = r_{\text{k}} + t$$

The thickness of the adsorbed layer can be evaluated experimentally with a non-porous silica [31] or less accurately calculated from different formula as De Boer equation:

$$t = \left(\frac{13.99}{0.034 - \log(p/p_0)}\right)^{0.5}$$

This represents the BJH method, which has been shown to underestimate the pore diameter by 20% for hydrophilic silica. This is due to the fact that in Kelvin equation the surface tension has been taken as a constant and it is in fact depending on the curvature of the pores for pore diameter inferior to 30 nm [24]:

$$\gamma = \gamma_\infty \left(1 - \left(\frac{0.66}{r_k}\right)\right)$$

where r_{k} is expressed in nm and γ_∞ is the surface tension measured for a flat infinite surface.

The BJH method with surface tension correction is in good agreement with the results found by the BdB method [13].

To evaluate precisely the size and the shape of the mesopores in hierarchical silica monoliths, geometrical pores diameter assuming spherical or cylindrical pores ($6V/S$* or $4V/S$*), respectively, have been compared to the pore sizes determined from the average pressures of the steps of the adsorption branch (by applying BdB desorption) for spherical pores and of the desorption branch (by applying BdB desorption) for cylindrical pores, respectively (Figure 8). In Figure 8, values of $6V/S$ and $4V/S$ have been included for comparison (open markers in Figure 8). For silica monoliths with different mesopores diameters, the best fit between capillary condensation pressures and geometrical calculations have been obtained for $6V/S$* revealing that the mesopores in silica monolith are of spherical shape with cavities sizes from 4 to 26 nm. This shape corresponds to the lowest diffusion properties of molecules into a material (see Section 2.1.3).

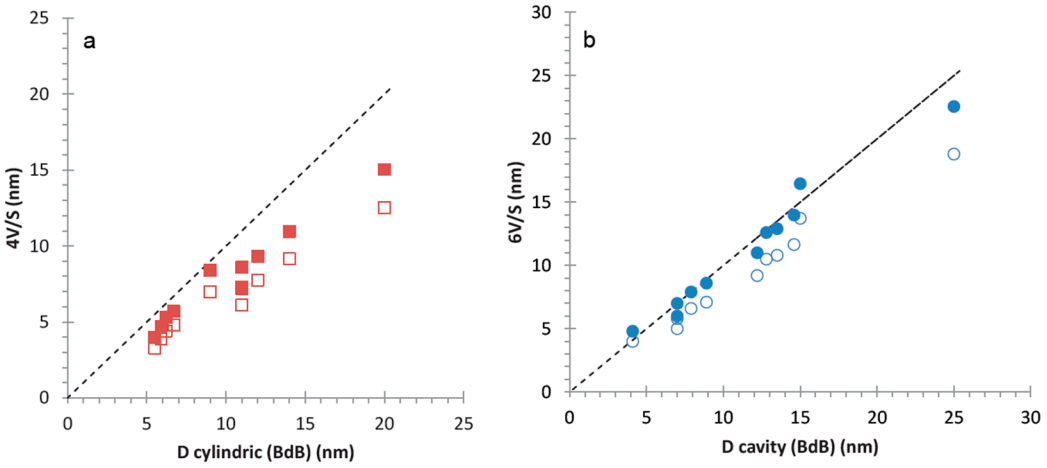

Figure 8. Comparison of mesopore diameters of hierarchical silica monoliths calculated by the geometrical method (**a**) $4V/S$ for cylindrical pore hypothesis and (**b**) $6V/S$ for spherical pore hypothesis (open square $4V/S$, plain square $4V/S$*, open circle $6V/S$, plain circle $6V/S$*) and mesopore diameters determined by the pressure of capillary condensation with the BdB method as explained in Figure 7.

To increase diffusion, cylindrical pores are needed. In order to form mesopores with cylindrical shape, the second alkaline step (NH_4OH treatment) of the monolith preparation was modified by replacing ammonia by a surfactant-templating agent (cetyltrimethyl ammonium bromide in NaOH solution) to form a MCM-41 like mesoporosity. The resulting nitrogen isotherm at 77 K (Figure 9) is characteristic of MCM-41 like mesoporosity with a sharp step in adsorption revealing uniform pores of 3.7 nm of diameter, a surface area of 1017 m^2/g and a pore volume of 0.86 mL/g. XRD pattern shows one peak at 2 θ around 2° (Figure 9) corresponding to a cell parameter a_0 of 4.85 nm and a wall-thickness of 1.1 nm with a second large peak usually found for worm-like structure of pores. TEM pictures show that some portions of the monolith are in hexagonal organization as expected for MCM-41 (Figure 9), but also some wormlike domains. In order to increase the mesopore diameter, a swelling agent 1,3,5-trimethylbenzene (TMB) was added to the synthesis medium and pores of 5.5 and 6.6 nm have been obtained by increasing the TMB amount (Figure 9). The shape of the pores has been checked as previously by comparing geometrical calculations ($4V/S$ and $6V/S$) to the pressure of capillary condensation using BdB method (Figure 10). The more accurate correlation is obtained for $4V/S$ ratio in accordance with cylindrical pores. However, due to the hydrophilic surface of the materials (C_{BET} = 90–100) it is surprising that the correlation is not $4V/S$* as usually found for MCM-41 prepared from silica alkoxide or silica powder (Table 1) [13]. The same feature is observed for other ordered mesoporous surfactant-templating silica powders such as HMS [32] with a worm-like structure and MCM-48 [33] with a cubic structure featuring both cylindrical pores with interconnections between pores (Table 1). The interconnections in a porous material add supplementary volumes in comparison to independent cylindrical pores, which false the geometrical calculation of cylindrical pores. By taking into account the mesopore diameter obtained by BdB method, the volume of the cylindrical pores and the volume of the connections can be evaluated (Table 2):

$$D_{cyl(BdB)} = 4V_{cyl}/S*$$

$$V_{cyl} = D_{cyl(BdB)}\, S*/4$$

$$V_{connec} = V - V_{cyl}$$

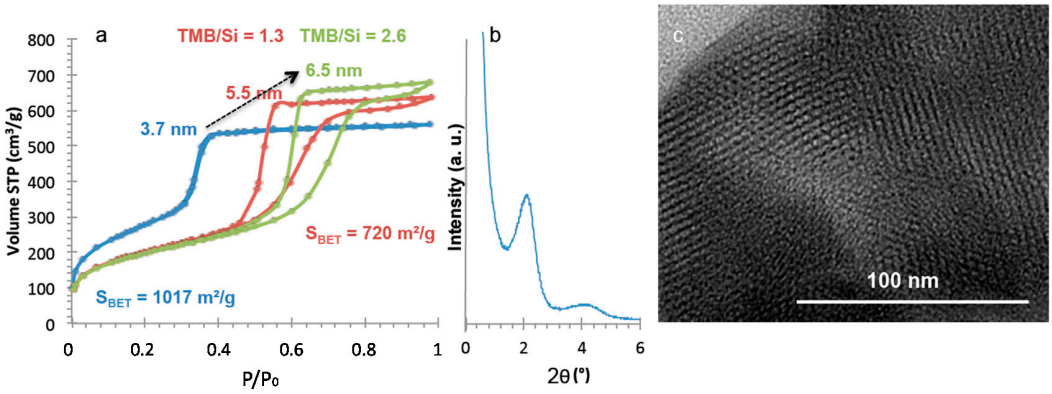

Figure 9. (**a**) Nitrogen sorption isotherms of calcined MCM-41-like hierarchical monoliths prepared with and without TMB (1,3,5-trimethylbenzene) as swelling agent; (**b**) XRD pattern; and (**c**) TEM picture of MCM-41-like hierarchical monolith prepared without TMB as swelling agent.

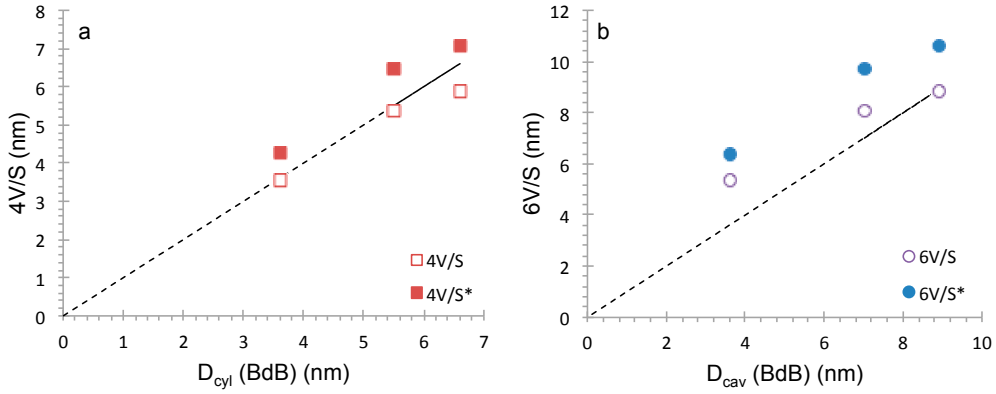

Figure 10. Comparison of mesopore diameters of MCM-41-like monoliths calculated by the geometrical method (**a**) $4V/S$ for cylindrical pore hypothesis and (**b**) $6V/S$ for spherical pore hypothesis (open square $4V/S$, plain square $4V/S$*, open circle $6V/S$, plain circle $6V/S$*) and mesopore diameters determined by the pressure of capillary condensation with the BdB method as explained in Figure 7.

Table 1. Textural properties of "classical" ordered mesoporous powders synthesized from Aerosil (MCM-41, MCM-48) or TEOS (HMS) as silica source.

Materials	V (mL/g)	S (m^2/g)	D_{cyl}(BdB) (nm)	$4V/S$ (nm)	$4V/S$* (nm)	$6V/S$ (nm)	$6V/S$* (nm)
MCM-41	0.67	890	3.7	3.0	3.6	4.5	5.4
MCM-41 [a]	1.90	830	10.4	9.1	11.0	13.7	16.4
MCM-48	0.99	1160	3.6	3.4	4.1	5.1	6.1
HMS	1.03	821	4.8	5.0	6.0	7.5	9.0

[a] MCM-41 swelled with TMB.

Table 2. Cylindrical and connection pores volumes of MCM-41-like Monoliths and as comparison of MCM-48 and HMS ordered mesoporous materials.

Materials	V_{total} (mL/g)	V_{cyl} (mL/g)	V_{connec} (mL/g)	V_{connec}/V_{total} (%)
MCM-48	0.99	0.87	0.12	12
HMS	1.03	0.82	0.21	20
Monolith MCM41	0.86	0.78	0.08	9
Monolith MCM41(TMB1.3)	0.98	0.83	0.15	15
Monolith MCM41(TMB2.6)	1.01	0.89 *	0.12 *	12 *

* calculated for a spherical shape of pore.

In MCM-41 like monoliths, the volume of interconnections represent 10%–15% of the total volume, which is close to MCM-48 materials (12% of total pore volume) and slightly below HMS materials revealing the highest degree of connectivity (20% of total pore volume) (Table 2). MCM-41-like Monolith synthesized with the higher amount of TMB possess pores with spherical shape and interconnections (12% of total pore volume) as observed in the correlation in Figure 10. MCM-41 like monoliths are therefore highly suitable for fast diffusion application. In summary, if silica materials are hydrophilic (C_{BET} = 90–100) and the correlation with geometrical calculation is closer to $4V/S$ or $6V/S$, it is an indication of interconnectivity in the material. These calculations may constitute therefore an original, simple and reliable method to determine the degree of mesopores connectivity in materials.

2.1.5. Mechanical Strength of Hierarchical Silica Monolith

The mechanical strength of a material is also a crucial parameter to be considered for its use in different applications, especially when the materials are highly porous like silica monoliths. Bending and compression tests have been performed on a silica monolith featuring mesoporous cavities of 16 nm with a mesopore volume of ~1 mL/g, a surface area of 700 m^2/g (organization of 4 nm nanoparticles), and a macropore volume of ~2 mL/g corresponding to a density of 0.28 g/cm^3. The hierarchical silica monolith shows a flexural strength of 0.96 MPa (standard deviation (s.d.) $\pm$0.17) and a compressive strength of 2.67 MPa (s.d. $\pm$0.32). The ratio of compressive strength over bending strength of ~2.8 lies in the typical range for brittle materials, most often between 2.5 and 10 [34]. Hierarchical silica monoliths have a mechanical strength lying between those of cork and balsa, as schematically represented on the strength–density chart of Figure 11. With such mechanical resistance macro-/mesoporous silica are therefore suitable for many applications such as catalysis or adsorption under continuous flow, as already demonstrated [1], but other applications could be envisaged such as thermal insulation, in which usually aerogels (purely mesoporous) are used [35]. Indeed hierarchical silica monoliths have a similar density as aerogels and similar compressive strengths [35]. Hierarchical silica monoliths could be used as model materials to test the influence of macropores in thermal insulators.

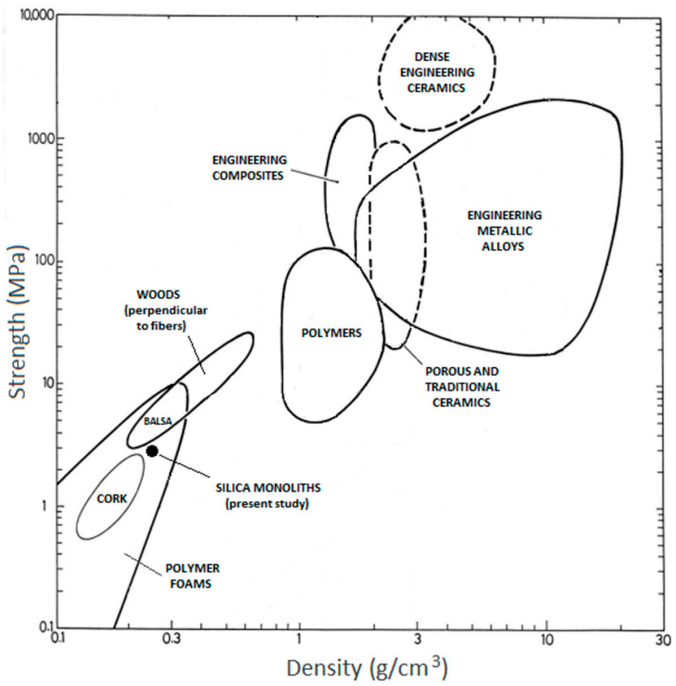

Figure 11. Comparison of the hierarchical silica monoliths of the present study (black bullet) with different classes of materials in a strength–density chart. Following Ashby's representation [34], "strength" stands for either compressive strength (brittle materials), tensile strength (composites) or yield stress (metals).

2.2. Mesoporous Silica Monoliths

In some applications as super thermal insulation mentioned above, monoliths featuring only mesoporosity are used. These monoliths are based on aerogels synthesized by sol-gel process followed by supercritical drying and feature mesopores in the range 20–50 nm. Aerogels have many fascinating properties such as high surface area (500–1000 m^2/g), high porosity (0.80–0.99), low bulk density (0.003–0.80 g/cm^3) and low thermal conductivity. Silica aerogels with densities of 0.15 and 0.28 g/cm^3 and compressive strengths of ~1 MPa exhibit a thermal conductivity of 13 and 23 mW/mK, respectively [35]. For 20 years efforts have been done to replace supercritical drying by room temperature and ambient pressure drying. Supercritical drying is not only expensive but also dangerous and difficult to industrialize [2]. The drying of the wet alcogels is the most important step in the synthesis of aerogels. Drying is governed by capillary pressure and the shrinkage of the gels during drying is driven by the capillary pressure, which may rich 100–200 MPa and lead to cracks in the monoliths. Organic alkoxide silanes have been largely used in post-treatment of alcogels to hydrophobize the surface and decrease capillary pressure by decreasing the surface tension of water at the surface of the pore [3]. Successful ambient pressure drying of aerogels has been realized. Herein, we present a new alternative to synthesize aerogels-like monoliths by using alkyl-polyethylene polymer without additional organosilane and using an ambient drying procedure.

Crack-free mesoporous silica monoliths, were obtained by using a short-chain PEO polymer (6.6 kDa) functionalized by a small hydrophobic chain containing nonyl chains and a phenyl group (EO_{150}-Phenyl-$(C9)_2$) to withstand the capillary forces exerted upon the framework during room temperature drying. This polymer is named Polyoxyethylene (150) dinonylphenyl ether (IGEPAL® DM-970, $(C_9H_{19})_2C_6H_3(C_2H_4O)_{150}OH$, M = 6944 g/mol). The synthesis was performed at higher temperature (100 °C) than the one used in previously described syntheses in order to increase the gelation rate and therefore favor the formation of mesopores (<50 nm) instead of macropores. Purely mesoporous silica monoliths have been obtained by avoiding macroscopic phase separation or precipitation within the gel for molar compositions of: 1 SiO_2/0.013 DM-970/ y H_2O/2.79 H_2SO_4 (y = 178, 50). This composition corresponds to EO unit/Si molar ratio of 1.95, which is higher than that used in the conditions of spinodal decomposition leading to macro/mesoporous monoliths (EO unit/Si = 0.60). For an amount of water corresponding to y = 20 H_2O a macroscopic phase separation is visible leading to additional spherical macropores of 30 microns (Figure 12). Lower amounts of water (y = 15, 10 H_2O), resulted in a phase separation leading to inhomogeneous macropores formation and monoliths breakage during calcination (not shown). The monoliths prepared with y = 178, 50 and 20 H_2O are named AN001, AN003 and AN004, respectively (Table 3) and are all cracks-free after drying and calcination at 550 °C.

Table 3. Textural properties of mesoporous silica monoliths.

Materials	V (mL/g)	S (m^2/g)	D_{cyl}(BdB) (nm)	D_{cav}(BdB) (nm)	4V/S (nm)	4V/S* (nm)	6V/S (nm)	6V/S* (nm)
AN001C [a]	1.18	628	16	20	7.5	9.0	11.3	13.5
AN003C [a]	1.54	885	10.5	12.4	7.0	8.3	10.4	12.5
AN004C [a]	1.07	575	11.2	15	7.4	8.9	11.1	13.4
AN001W [b]	3.67	1201	27	28	12.2	14.7	18.3	22

[a] C: calcined at 550 °C; [b] W: washed with H_2O/EtOH.

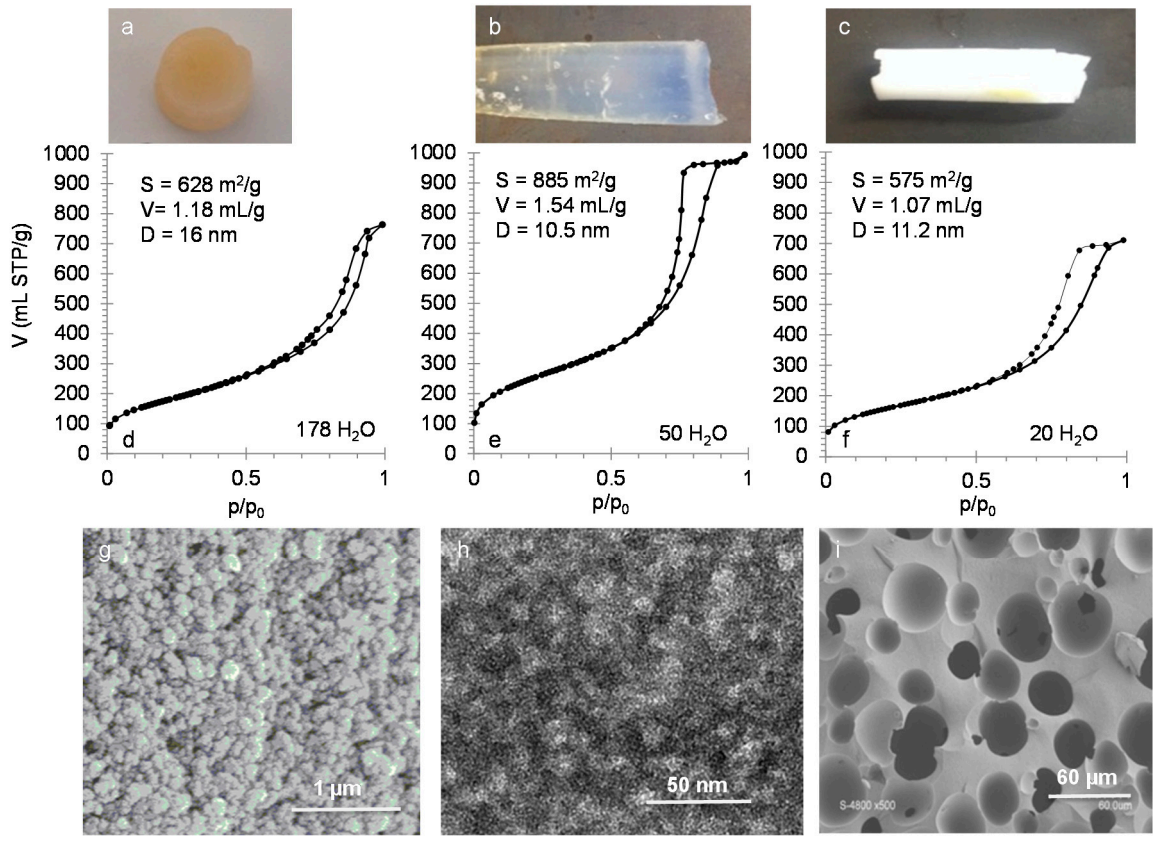

Figure 12. (**a**–**c**) Characteristic images of the monoliths prepared with high amounts of water (50 and 178 H_2O): (**b**) transparent after synthesis and (**a**) opaque after calcination, and (**c**) low amount of water (20 H_2O, white). (**d**–**f**) Nitrogen sorption isotherms at 77 K of calcined mesoporous silica monoliths (aerogels-like materials) prepared with different amount of water. (**g**–**i**) SEM images of monoliths prepared with 178 (**g**) and 20 H_2O (**i**) and TEM picture of monolith prepared with 50 H_2O (**h**).

After synthesis the monoliths were transparent (except for the synthesis with 20 H_2O, which produced a white material) and after calcination the monoliths turned opaque (except for the synthesis with 20 H_2O, which remained white) and no cracks were visible (Figure 12). After calcination at 550 °C, these monoliths feature a surface area in the range 600–800 m^2/g, a high mesopore volume 1.1–1.5 mL/g and mesopore sizes between 10 and 16 nm (BdB desorption applied to desorption branch) (Table 3). The monolith prepared with the highest amount of water (y = 178 H_2O) present a granular-like silica structure (SEM in Figure 12) as classically found in commercial aerogels [36]. The monolith is formed by an aggregation of silica nanoparticles of 60–120 nm, leading to mesopore sizes from 25 to 60 nm, with the presence of larger pores around 100 nm (SEM in Figure 12). Nitrogen adsorption isotherm of this monolith only identified the mesopores below 50 nm, the largest ones being filled at p_0 and not below. Decreasing the amount of water from y = 178 to 50 H_2O in the synthesis mixture decreased the mesopore diameter to 10–15 nm (white spots in TEM in Figure 12) in accordance with nitrogen adsorption results. The size of the silica nanoparticles forming the monolith structure is of the same order of magnitude according to TEM pictures (black spots in TEM in Figure 12). In acidic medium, decreasing the water content decreases the pH of the solution and increases silica concentration, which favor a faster gelation of silica. More silica nuclei will be present initially in the solution and more particles will be formed, which does not further increase in size. For a lower amount of water (y = 20 H_2O), a lower pH allows the formation of even smaller silica nanoparticles and a continuous phase of silica/polymer can form, which is responsible for a phase separation process with a water rich phase. In the present case, the phase separation is not bicontinuous as previously described

for spinodal decomposition, but leads to spherical macropores in the silica structure. The presence of macropores is responsible for the white color of the monolith as it decreases the optical transmission by promoting light scattering.

To determine the shape of the mesopores in these monoliths, geometrical calculations were performed and compared to mesopore sizes determined by the capillary condensation pressures (Table 3). The mesopores are of spherical shape as a closer relationship is found for $6V/S^*$. The correlation is not accurate for the mesoporous monolith prepared with the highest amount of water (AN001C, y = 178 H_2O), which is due to the fact that the some mesopores are too large to be entirely filled by nitrogen below p_0. A pore volume higher than 1.18 mL/g should be considered. It is to notice that the nanoparticle sizes measured in SEM pictures (60–120 and 10–15 nm for AN001C and AN003C, respectively) are much larger than the ones calculated from the surface area of the materials with the relation $d = 6/S\rho$ (4.3 and 3.1 nm, respectively) (see Section 2.1.3) suggesting that the silica nanoparticles may contain also micropores or small mesopores. The microporosity could arise from the penetration of the polyethylene chains into the silica network, which after calcination gives rise to micropores as it is the case for SBA-15 materials [37]. Solvents extraction of the polymer before calcination were performed with as-synthesized monolith AN001 (y = 178 H_2O) with 2-propanol or acetone at 40 °C for 24 h (4 times), which resulted in monoliths (S = 615 m^2/g, V = 1.4 mL/g) which present some cracks after washing, but evidence, in addition to large mesopores of 22 nm, the presence of small mesopores around 4 nm (presence of a large step in nitrogen adsorption between $0.4 < p/p_0 < 0.5$ with a volume of 100 mL STP height, not shown). The condensation state of silica in acidic medium is low and the calcination should have led to a restructuration the small mesoporosity towards a broader distribution of mesopore sizes, which becomes barely visible on nitrogen sorption of calcined monoliths. A more gentle solvent extraction of the polymer was performed by using water and then successive ethanol/water washings with increasing amounts of ethanol to end with pure ethanol washing leading to a crack-free monolith after drying. Water washing alone was not effective enough to remove the polymer for all monoliths, resulting in monoliths with very low surface area (50–150 m^2/g) and pore volumes (0.2–0.5 mL/g) (as exemplified in Figure 13). After the washings with EtOH gradients, the silica monolith (AN001W) exhibited a very high surface area (1201 m^2/g), a very high mesopore volume (3.65 mL/g) and a mesopore diameter around 30 nm. However the presence of small mesopores is barely visible (Figure 13), some restructuration of the small mesoporosity should have occurred during this washing. TEM pictures performed on the calcined monolith confirm the presence of two phases in the monolith: an aggregation of particles of *ca.* 40 nm giving rise to large mesopores and larger nanoparticles (300 nm) containing ordered small mesoporosity (Figure 14).

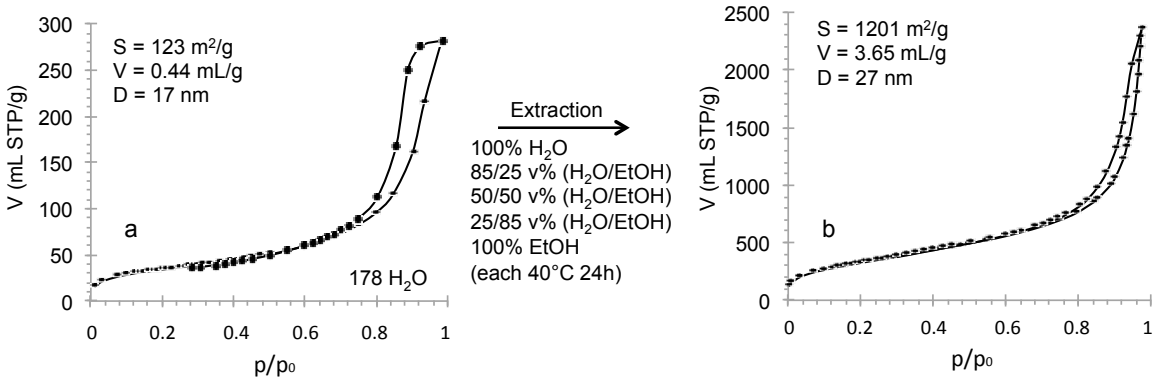

Figure 13. Nitrogen sorption isotherms at 77 K of as-synthesized (**a**) and solvent-extracted (**b**) mesoporous silica monoliths (aerogels-like materials) prepared with 178 H_2O and high amount of surfactant-polymer DM-970.

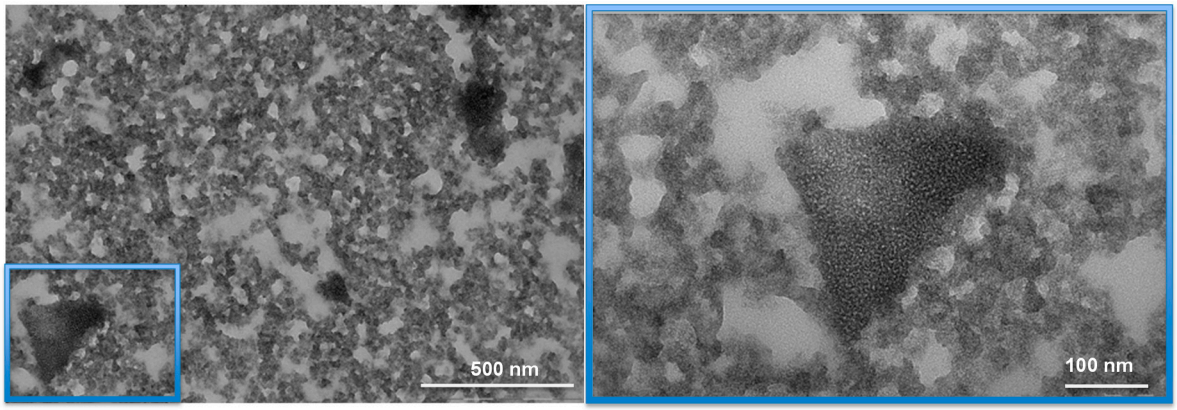

Figure 14. TEM pictures at two different magnifications of calcined mesoporous silica monoliths (AN001C) prepared with 178 H_2O and high amount of surfactant-polymer DM-970.

As a first preliminary step to understand the formation of these new mesoporous monoliths, we noticed that decreasing the amount of polymer DM-970 (EO_{150}-Phenyl-$(C9)_2$) in the synthesis resulted in the precipitation of the gel and the existence of a different mechanism of porous silica formation. Instead of nanoparticles formation or phase separation mechanisms as described above, a surfactant-templating mechanism takes place and ordered mesoporous silicas were obtained (Figure 15). This suggests that lowering the amount of polymer allows the interactions of the hydrophobic chain of the PEO polymer. Ordered mesoporous silica materials were obtained for a molar composition of the gel: 1 SiO_2/0.0065 DM-970/178 H_2O/2.79 H_2SO_4. The composition of the synthesis medium corresponds to an EO unit/Si molar ratio of 0.97 instead of 1.95. A lower amount of polymer favors the condensation of silanol groups, which is the driving force for a self-assembly mechanism and the formation of silicate-surfactant micelles. XRD patterns and TEM images suggest a worm-like structure with a correlation distance between pores around 7 nm (Figure 15). After calcination, the material features a high surface area of 1321 m^2/g, a pore volume of 0.75 mL/g and a mesopore diameter around 3 nm (with a distribution of pores between 2 and 4 nm) (Figure 14). The surface area of these new ordered mesoporous materials is not consistent with a wall thickness (t) of 3–4 nm determined by TEM. Indeed for hexagonal mesoporous solids it was shown [38] that the surface area is equal to:

$$S\,(m^2/g) \;=\; 2000/\rho t$$

where ρ is the silica density (2.2 g/cm^3) and the thickness, t, is in nm.

This suggests a restructuration of the small mesopores into a broader size distribution during the calcination or the presence of micropores in the walls due the ethylene oxide chain penetration. A mesopore diameter of 3 nm corresponds to twice the length of the hydrophobic chain of the polymer, evidencing that the hydrophobic part of the polymer is in the center of the mesopores and the hydrophilic PEO chains are in the silica walls as for SBA-15 materials synthesized with shorter ethylene oxide chains (EO_{20}-PO_{70}-EO_{20}) (EO unit/Si = 0.68) surfactant [37]. After water washing, a material with the same pore size as the calcined one and a surface area of 411 m^2/g is obtained. This suggests a higher state of condensation of the silica as a part of the polymer could be removed. The mesopore diameter is close to the value calculated via the $4V/S^*$ (2.7 nm) geometrical calculation suggesting that mesopores have a cylindrical geometry and no connections. Further investigations on this new type of mesoporous materials are under study.

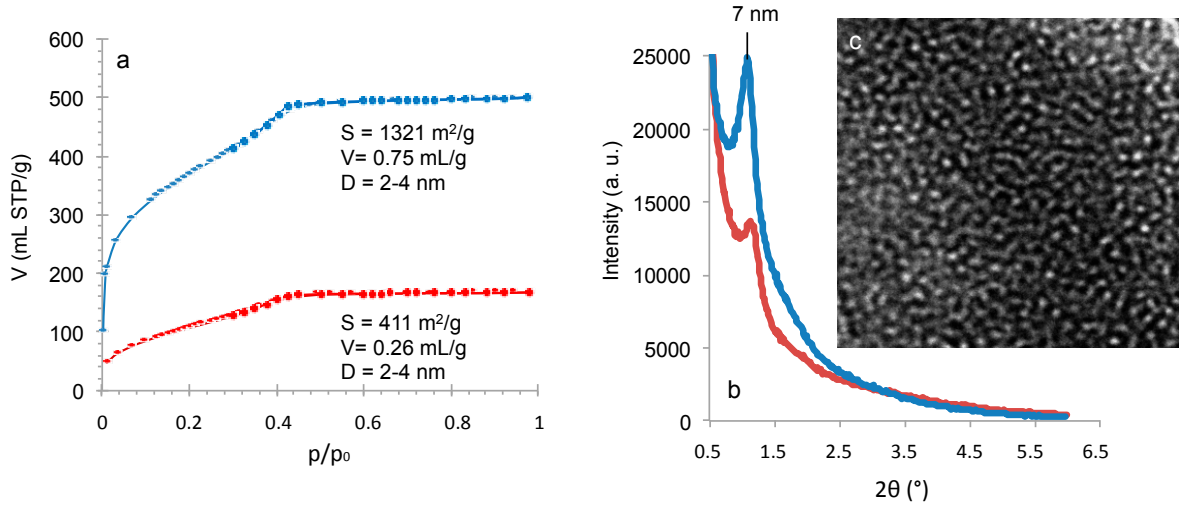

Figure 15. (**a**) Nitrogen sorption isotherms at 77 K, (**b**) XRD pattern and (**c**) TEM image of as-synthesized (red) and calcined (blue) worm-like mesoporous silica powders prepared with 178 H_2O and low amount of surfactant-polymer DM-970.

A possible representation of these new mesoporous silica materials, monoliths build of silica nanoparticles and ordered mesoporous powder is represented schematically in Figure 16. Polyethylene polymer interacts strongly with silica species by H-bonding. In the case of high amount of polymer (DM-970), large silica /polymer nanoparticles are formed, with the alkyl chains at the surface contributing to their stabilization into aggregates (Figure 16). The large size of the silica nanoparticles (40 nm) prevents the alkyl chain to interact to form micelles. A lower amount of water in the synthesis increases the pH and the silica concentration, which leads to smaller silica nanoparticles (10 nm), but these particles are large enough to prevent micelles formation. A lower amount of polymer leads to smaller silica/PEO complexes (1–3 nm), which form smaller head groups for the surfactant-polymer and allow the hydrophobic chains to interact to form micelles leading under condensation and self-assembly mechanism to ordered mesoporous materials. It is to notice that not only the polymer and water amounts control the formation of stable mesoporous monolith, but also the choice of the acid. By replacing H_2SO_4 by HCl in the synthesis, cracks were observed before washing and drying. Sulfate anions also contribute to the stability of the mesoporous monoliths.

These new mesoporous monoliths may constitute an original family of crack-free silica monoliths similar to aerogels prepared via ambient drying without using surface modifiers such as alkoxysilanes thanks to the intrinsic hydrophobic character of the final chain of the polymer. Further studies should be envisaged to understand the formation of these mesoporous monoliths and comparison of these new mesoporous silica monoliths and meso-/macroporous monoliths with aerogels in thermal insulation applications should be considered.

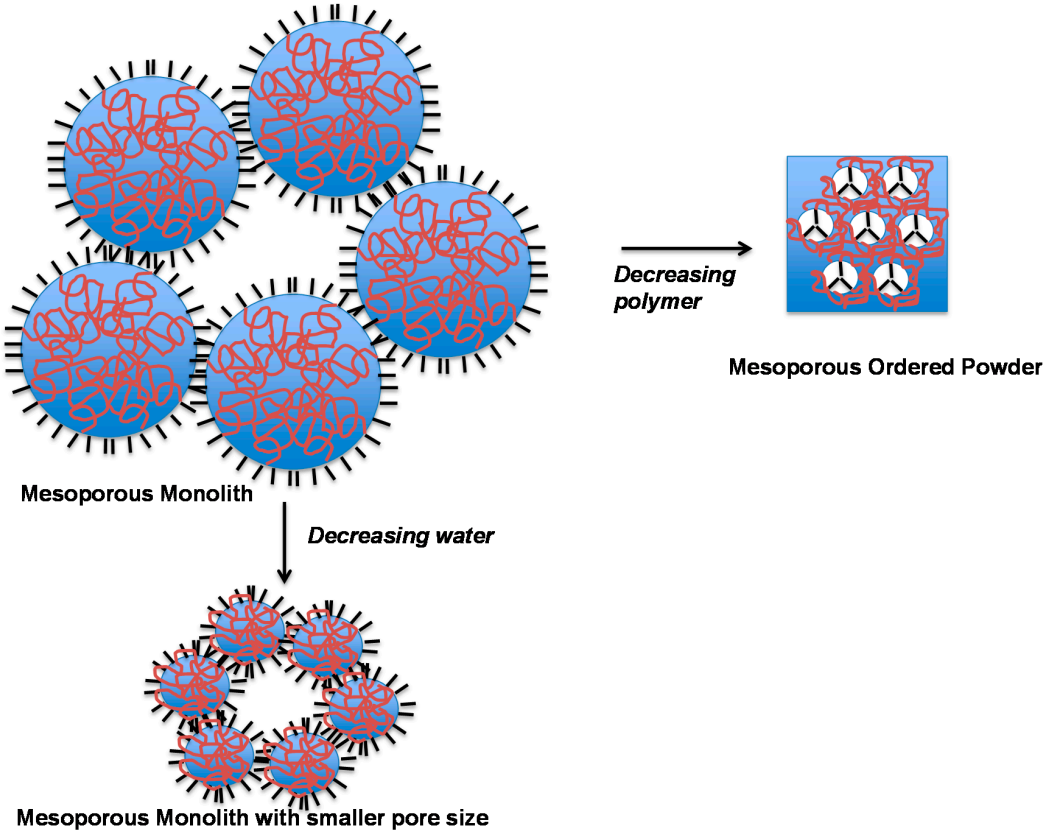

Figure 16. Schematic representation of the mesoporosity of the materials: mesoporous monoliths or ordered mesoporous powder as a function of polymer (DM-970) amount and water content. Blue is for silica, Black is the alkyl chain of the polymer, Red is the EO chain of the polymer.

3. Experimental Section

3.1. Synthesis of Macroporous Silica Monoliths with Disordered Mesoporosity

A very precise amount of tetraethylorthosilicate (TEOS, Aldrich, Steinheim, Germany) (20 g) is weighted and left at −19 °C for 1 h. In a 100 mL Erlenmeyer flask, water (24.560 g) is precisely weighed and then (2.313 g) nitric acid (68%) is added. The mixture is stirred 5 min at room temperature. A precise amount (2.534 g) of polyethylene oxide (PEO) (20 kDa) is weighed, added to the mixture and stirred at room temperature until having complete dissolution of the polymer. The mixture is left for 10 min at −19 °C in the freezer to cool down the solution without freezing. The flask is then placed in an ice bath well surrounded by ice, stirred. TEOS (coming from the freezer) is directly added to the slurry and the solution is stirred for 30 min. The final composition of the mixture in molar ratio is: 1 Si/0.60 EO/0.26 HNO_3/14.21 H_2O. Eight Polyvinyl chloride (PVC) tubes of 8 mm diameter and 10 cm length are closed on one side with a cap, sealed with parafilm and kept at −19 °C in the freezer. The tubes are taken from the freezer and filled with the mixture of the ice bath. The tubes are then closed by caps and sealed with parafilm and left in 4 L water bath at 40 °C for 3 days. The phase separation and the sol-gel process take place, monoliths are forming resulting in 1 mm shrinkage around the section of the monolith. Monoliths are then removed from the tube molds and placed in 1 L water bath at room temperature. Water is changed every 30 min until reaching a neutral pH (around 5 washing). The monoliths are then immersed in 1 L aqueous ammonia (0.1 M) in a polypropylene bottle and left in an oven at 40 °C for 1 day. Resulting monoliths are placed in a water bath and water is changed every 30 min until neutral pH (washing around three time). The monoliths are then dried at room temperature for 4 days and calcined at 550 °C for 8 h under air to remove remaining PEO.

3.2. Synthesis of Macroporous Silica Monoliths with Ordered Mesoporosity

MCM-41-like monoliths syntheses were adapted from previous work [9]. Silica monoliths obtained after the phase separation and sol-gel process (first step in acidic medium) are taken from the neutral water bath and reacted in an alkaline solution containing water, NaOH (Aldrich) and cetyltrimethylammonium bromide (CTAB, Aldrich). In a typical synthesis, two wet monoliths (2×10 cm, corresponding to 0.80 g each of dried and calcined SiO_2) are taken and placed at the bottom of an autoclave. An aqueous solution is prepared by dissolving 0.213 of NaOH in 192 g of water. Then, 5.831 g of CTAB are added and the mixture is stirred for 1 h at room temperature. Eventually, 2.083 or 4.16 g of 1,3,5-trimethylbenzene (TMB, Aldrich) is added to swell the micelles and enlarged the pores. The alkaline solution is poured on the autoclave containing the monoliths and left in an oven at 115 °C for 6 days. The final composition in molar ratio is: 1 Si/0.60 CTAB/0.2 NaOH/400 H_2O/ x TMB (x = 0, 1.3, 2.6). Monoliths are then removed from the autoclave and placed in 1 L water bath at room temperature. Water is changed every 30 min until reaching a neutral pH (around 3 washing). Monoliths are then dried at 80 °C for 1 day and calcined at 550 °C for 8 h under air to remove CTAB and remaining PEO.

3.3. Synthesis of Mesoporous Silica Monoliths

Polyoxyethylene (150) dinonylphenyl ether (IGEPAL® DM-970, $(C_9H_{19})_2C_6H_3(C_2H_4O)_{150}OH$, M = 6944 g/mol), tetraethylorthosilicate (TEOS), and sulfuric acid (H_2SO_4, 98%) were obtained from Sigma-Aldrich. An aqueous solution of polymer-surfactant was first prepared by mixing 4 g of DM-970 with x g H_2O (x = 138, 39, 15 g) and 12.2 g H_2SO_4 (37%). The mixture was stirred for 60 min. Then TEOS (9 g) was added to the mixture and left under stirring for 24 h at room temperature. The resulting molar ratio is (AN001, 003, 004) 1 SiO_2/0.013 DM-970/y H_2O/2.79 H_2SO_4 (y = 178, 50, 20). This composition corresponds to EO unit/Si molar ratio of 1.95. The mixture was then heated in Teflon lined stainless autoclave without stirring at 100 °C for 72 h. The resulting monolith was washed with water (400 mL for 24 h, 3 times), dried at 80 °C 12 h and calcined at 550 °C in air for 6 h. Instead of calcination, an extraction of the polymer was also performed by washing the monolith several times at 40 °C for 24 h with: 400 mL H_2O, 300 mL H_2O and 100 mL EtOH, 200 mL H_2O and 200 mL EtOH, 100 mL H_2O and 300 mL EtOH, 400 mL EtOH, followed by a drying at 80 °C 12 h.

3.4. Synthesis of Ordered Mesoporous Silica Powder

A similar procedure was repeated with 2 times less DM-970. An aqueous solution of polymer-surfactant (cmc = 0.002 mol/L) was first prepared by mixing 2 g of DM-970 with 30 g H_2O and 120 g H_2SO_4 (2 N). The mixture was stirred for 60 min. Then TEOS (9 g) was added to the mixture and left under stirring for 24 h at room temperature. The resulting molar ratio is (ZA026) 1 SiO_2/0.0065 DM-970/178 H_2O/2.79 H_2SO_4. The mixture was then heated in Teflon lined stainless autoclave without stirring at 100 °C for 48 h. The resulting material was washed with water until neutral pH (400 mL for 24 h, 3 times), dried at 80 °C for 12 h and calcined at 550 °C in air for 8 h. This composition corresponds to EO unit/Si molar ratio of 0.97.

3.5. Materials Characterization

X-Ray Diffraction (XRD) patterns of the materials were performed using a Bruker D8 Advance diffractometer with a Bragg-Brentano geometry and equipped with a Bruker Lynx Eye detector (Brucker, Heidelberg, Germany). XRD patterns were recorded in the range 1°–6° (2θ) to identify MCM-41 like peaks. The angular step size was of 0.0197° and the counting time of 0.2 s per step. The textural properties of the materials were determined from the N_2 adsorption/desorption isotherms at 77 K measured on a Micromeritics Tristar 3000 apparatus (Micromeritics, Verneuil Halatte, France). The samples were previously outgassed in vacuum at 250 °C for 12 h. The mesoporous volume was taken at the end of the capillary condensation steps. The surface area was calculated by the

Brunauer–Emmett–Teller (BET) method. The mesopore diameter was estimated using the desorption branch of the isotherm and using the Broekhoff and de Boer method, as it has been previously demonstrated as one of the most accurate method for mesopore size determination for hydroxylated silica materials [39]. The morphology of the monoliths was studied using a Hitachi S-4800 I scanning electron microscope (SEM) and by transmission electron microscopy (TEM) using a JEOL 1200 EXII instrument at "Plateau Technique Pole Chimie Balard Montpellier" (France). The flexural strength was measured in three-point bending on monoliths of ~6 mm in diameter with spans between ~20 mm and 32 mm. Compression tests were made on monoliths of ~6 mm in diameter and ~12 mm in height that had been cut out from a monolith of 10 cm length.

4. Conclusions

Silica monoliths with hierarchical macro-/mesoporosity (prepared by spinodal decomposition between a polyethylene/silica rich phase and a water rich phase) are outstanding materials for continuous flow processing of liquids in catalysis, adsorption and separation. Pressure drop is an important parameter for process intensification and industrialization, and should be minimized. Pressure drop of these macro-/mesoporous monoliths depends on macropore size and can be adjusted to the demands posed by specific applications. A relationship between pressure drop and macropore size has been established in this study and can be used to predict the drop pressure for different liquids by adjusting the viscosity of the liquid in the new equation. We have shown that the permeability of the hierarchical macro-/mesoporous monoliths is close to the permeability of cylindrical channels although their macropore architecture is more complex, but is however totally interconnected and uniform. The internal mass transport of molecules to and from the active centers is also very important to accurately control the contact time of a reaction, the internal diffusion limitation and therefore the intrinsic rate of the reaction. The internal mass transport is controlled by the architecture of the mesopores and is determined by the size, the shape, and the connectivity of the pores. Methodologies to identify these parameters have been presented in this study and for the first time a possible way to quantify interconnections in between silica mesopores is given. The highest internal diffusion (or internal mass transport) was obtained for cylindrical interconnected mesopores. Finally, a new synthesis procedure allowing to form purely mesoporous silica monoliths (aerogel-like materials without the use of supercritical drying or post-modification by organosilane) largely developed for applications as super thermal insulator has been presented using an alkyl-polyethylene polymer. Depending on the amount of water the mesopore diameters can be adjusted between 10 and 30 nm. Mesoporous silica monoliths with surface areas as high as 1300 m^2/g and pore volumes as high as 3 mL/g have been obtained. Interestingly, decreasing the amount of polymer gives rise to the precipitation of a new kind of ordered mesoporous material (wormlike structure) with 3 nm mesopores and 4 nm wall-thickness and a surface area of *ca.* 1300 m^2/g.

Complete methodology to characterize mesoporous silica materials have been presented in this study as well as recipes to form either mesoporous monoliths or meso-/macroporous monoliths using polyethylene oxides-based polymer and silica.

Acknowledgments: This research was funded by the Agence Nationale de la Recherche ANR (French National Research Agency): Project Labex CheMIsyst (ref. ANR-10-LABX-05-01), Project ANR-TAMTAM (ref. ANR-15-CE08-0008-01). Authors thank Didier Cot and Thomas Cacciaguerra for SEM analysis. Anne Galarneau thanks Elisabeth Charlaix and Cyril Picard for fruitful discussions. Katarzyna Szymanska and Andrzej Jarzębski thank the National Science Center of Poland for the support, Grant No UMO-2013/09/B/ST8/02420.

Author Contributions: Anne Galarneau: Writing the manuscript and the discussion of the results; Zakaria Abid: Mesoporous silica monolith synthesis; Bilel Said: Hierarchical silica monolith synthesis; Youcef Didi: MCM-41-like monolith synthesis; Katarzyna Szymanska and Andrzej Jarzębski: Drop pressure measurements and discussion; Franck Tancret: Mechanical tests measurements and discussion; Hadj Hamaizi, Abdelkader Bengueddach, and Francesco Di Renzo: Raise funding for Zakaria Abid to come to France; Francois Fajula: Discussions and corrections of the manuscript.

Conflicts of Interest: The authors declare no conflict of interest.

References

1. Galarneau, A.; Sachse, A.; Said, B.; Pelisson, C.-H.; Boscaro, P.; Brun, N.; Courtheoux, L.; Olivi-Tran, N.; Coasne, B.; Fajula, F. Hierarchical porous silica monoliths: A novel class of microreactors for process intensification in catalysis and adsorption. *Comptes Rendus Chim.* **2016**, *19*, 231–247. [CrossRef]
2. Aravind, P.R.; Shajesh, P.; Soraru, G.D.; Warrier, K.G.K. Ambient pressure drying: A successful approach for the preparation of silica and silica based mixed oxide aerogels. *J. Sol Gel Sci. Technol.* **2010**, *54*, 105–117. [CrossRef]
3. Hwang, S.-W.; Jung, H.-H.; Hyun, S.-H.; Ahn, Y.-S. Effective preparation of crack-free silica aerogels via ambient drying. *J. Sol Gel Sci. Technol.* **2007**, *41*, 139–146. [CrossRef]
4. Guyomard-Lack, A.; Said, B.; Dupré, N.; Galarneau, A.; le Bideau, J. Enhancement of lithium transport by controlling the mesoporosity of silica monoliths filled by ionic liquids. *New J. Chem.* **2016**. [CrossRef]
5. Belmoujahid, Y.; Bonne, M.; Scudeller, Y.; Schleich, D.; Grohens, Y.; Lebeau, B. Thermal conductivity of monolithic assemblies of SBA-15 ordered mesoporous silica particles. *Microporous Mesoporous Mater.* **2015**, *201*, 124–133. [CrossRef]
6. Wei, T.-Y.; Chang, T.-F.; Lu, S.-Y. Preparation of monolithic silica aerogel of low thermal conductivity by ambient pressure drying. *J. Am. Ceram. Soc.* **2007**, *90*, 2003–2007. [CrossRef]
7. Inayat, A.; Reinhardt, B.; Uhlig, H.; Einicke, W.-D.; Enke, D. Silica monoliths with hierarchical porosity obtained from porous glasses. *Chem. Soc. Rev.* **2013**, *42*, 3753–3764. [CrossRef] [PubMed]
8. Nakanishi, K. Pore structure control of silica gels based on phase separation. *J. Porous Mater.* **1997**, *4*, 67. [CrossRef]
9. Babin, J.; Iapichella, J.; Lefevre, B.; Biolley, C.; Bellat, J.-P.; Fajula, F.; Galarneau, A. MCM-41 silica monoliths with independent control of meso- and macroporosity. *New J. Chem.* **2007**, *31*, 1907–1917. [CrossRef]
10. El Kadib, A.; Chimenton, R.; Sachse, A.; Fajula, F.; Galarneau, A.; Coq, B. Functionalized inorganic monolithic microreactors for high productivity in fine chemicals catalytic synthesis. *Angew. Chem. Int. Ed.* **2009**, *48*, 4969–4972. [CrossRef] [PubMed]
11. Triantafillidis, C.; Elsaesser, M.; Husing, N. Chemical phase separation strategies towards silica monoliths with hierarchical porosity. *Chem. Soc. Rev.* **2013**, *42*, 3833–3846. [CrossRef] [PubMed]
12. Sachse, A.; Galarneau, A.; Fajula, F.; di Renzo, F.; Creux, P.; Coq, B. Functional silica monoliths with hierarchical uniform porosity as continuous flow catalytic reactors. *Microporous Mesoporous Mater.* **2011**, *140*, 58–68. [CrossRef]
13. Cahn, J.W.; Hilliard, J.E. Free energy of a nonuniform system. I. Interfacial free energy. *J. Chem. Phys.* **1958**, *28*, 258. [CrossRef]
14. Cahn, J.W.; Hilliard, J.E. Free energy of a nonuniform system. III. Nucleation in a two-component incompressible fluid. *J. Chem. Phys.* **1959**, *31*, 688. [CrossRef]
15. Wiki. Available online: https://upload.wikimedia.org/wikipedia/commons/9/9b/CahnHilliard_Animation.gif (accessed on 10 February 2016).
16. Kim, S.Y.; Meyer, H.W.; Saalwachter, K.; Zukoski, C.F. Polymer dynamics in PEG-silica nanocomposites: Effects of polymer molecular weight, temperature and solvent dilution. *Macromolecules* **2012**, *45*, 4225–4237. [CrossRef]
17. Szymanska, K.; Pietrowska, M.; Kocurek, J.; Marez, K.; Koreniuk, A.; Mrowiec-Bialon, J.; WidlakMagner, P.; Jarzebski, E.A. Low back-pressure hierarchically structured multichannel microfluidic bioreactors for rapid protein digestion—Proof of concept. *Chem. Eng. J.* **2016**, *287*, 148–154. [CrossRef]
18. Whitaker, S. Advances in theory of fluid motion in porous media. *Ind. Eng. Chem.* **1967**, *12*, 14–28. [CrossRef]
19. Sachse, A.; Hulea, V.; Finiels, A.; Coq, B.; Fajula, F.; Galarneau, A. Alumina-grafted macro-/mesoporous silica monoliths as continuous flow microreactors for the Diels–Alder reaction. *J. Catal.* **2012**, *287*, 62–67. [CrossRef]
20. Galarneau, A.; Iapichella, J.; Brunel, D.; Fajula, F.; Bayram-Hahn, Z.; Unger, K.; Puy, G.; Demesmay, C.; Rocca, J.-L. Spherical ordered mesoporous silicas and silica monoliths as stationary phases for liquid chromatography. *J. Sep. Sci.* **2006**, *29*, 844–855. [CrossRef] [PubMed]
21. Chemmi, H.; Petit, D.; Levitz, P.; Denoyel, R.; Galarneau, A.; Korb, J.-P. Noninvasive experimental evidence of the linear pore size dependence of water diffusion in nanoconfinement. *J. Phys. Chem. Lett.* **2016**, *7*, 393–398. [CrossRef] [PubMed]

22. Ruckenstein, E.; Tsai, M.C. Optimum pore size for the catalytic conversion of large molecules. *AiChE J.* **1981**, *27*, 697. [CrossRef]
23. Rouquerol, J.; Llewellyn, P.; Rouquerol, F. Is the BET equation applicable to microporous adsorbents? *Stud. Surf. Sci. Catal.* **2006**, *160*, 49–56.
24. Gregg, S.J.; Sing, K.S.W. *Adsorption, Surface Area and Porosity*; Academic Press: London, UK; New York, NY, USA, 1982.
25. Martin, T.; Lefevre, B.; Brunel, D.; Galarneau, A.; Di Renzo, F.; Fajula, F.; Gobin, P.F.; Quinson, J.F.; Vigier, G. Dissipative water intrusion in hydrophobic MCM-41 type materials. *Chem. Commun.* **2002**, 24–25. [CrossRef]
26. Martin, T.; Galarneau, A.; Brunel, D.; Izard, V.; Hulea, H.; Blanc, A.C.; Abramson, S.F.; di Renzo, F.; Fajula, F. Towards total hydrophobisation of MCM-41 type silica surface. *Stud. Surf. Sci. Catal.* **2001**, *135*, 4621–4628.
27. Broekhoff, J.C.; de Boer, J.H.J. Studies on pore systems in catalysts: XIII. Pore distributions from the desorption branch of a nitrogen sorption isotherm in the case of cylindrical pores B. Applications. *J. Catal.* **1968**, *10*, 377. [CrossRef]
28. Coasne, B.; Galarneau, A.; di Renzo, F.; Pellenq, R.J.M. Effect of morphological defects on gas adsorption in nanoporous silicas. *J. Phys. Chem. C* **2007**, *111*, 15759–15770. [CrossRef]
29. Coasne, B.; Galarneau, A.; di Renzo, F.; Pellenq, R.J.M. Molecular simulation of adsorption and intrusion in nanopores. *Adsorption* **2008**, *14*, 215–221. [CrossRef]
30. Coasne, B.; Galarneau, A.; Pellenq, R.J.M.; di Renzo, F. Adsorption, intrusion and freezing in porous silica: The view from the nanoscale. *Chem. Soc. Rev.* **2013**, *42*, 4141–4171. [CrossRef] [PubMed]
31. Galarneau, A.; Villemot, F.; Rodriguez, J.; Fajula, F.; Coasne, B. Validity of the *t*-plot method to assess microporosity in hierarchical micro/mesoporous materials. *Langmuir* **2014**, *30*, 13266–13274. [CrossRef] [PubMed]
32. Galarneau, A.; Renard, G.; Mureseanu, M.; Tourrette, A.; Biolley, C.; Choi, M.; Ryoo, R.; di Renzo, F.; Fajula, F. Synthesis of sponge mesoporous silicas from lecithin/dodecylamine mixed-micelles in ethanol/water media: A route towards efficient biocatalysts. *Microporous Mesoporous Mater.* **2007**, *104*, 103–114. [CrossRef]
33. Galarneau, A.; Driole, M.-F.; Petitto, C.; Chiche, B.; Bonelli, B.; Armandi, M.; Onida, B.; Garrone, E.; di Renzo, F.; Fajula, F. Effect of post-synthesis treatment on the stability and surface properties of MCM-48 silica. *Microporous Mesoporous Mater.* **2005**, *83*, 172–180. [CrossRef]
34. Munz, D.; Fett, T. *Ceramics: Mechanical Properties, Failure Behaviour, Materials Selection*; Springer Verlag: Heidelberg, Germany, 1999; ISBN: 978-3-642-58407-7.
35. Wong, J.C.H.; Kaymak, H.; Brunner, S.; Koebel, M.M. Mechanical properties of monolithic silica aerogels made from polyethoxydisiloxanes. *Microporous Mesoporous Mater.* **2014**, *183*, 23–29. [CrossRef]
36. Caputo, G. Fixed bed adsorption of drugs on silica aerogel from supercritical carbon dioxide solutions. *Int. J. Chem. Eng.* **2013**, *2013*, 752719. [CrossRef]
37. Galarneau, A.; Cambon, H.; di Renzo, F.; Ryoo, R.; Choi, M.; Fajula, F. Microporosity and connections between pores in SBA-15 mesostructured silicas as a function of the temperature of synthesis. *New J. Chem.* **2003**, *27*, 73–79. [CrossRef]
38. Di Renzo, F.; Desplantier, D.; Galarneau, A.; Fajula, F. Thermal and mechanical stability of micelle-templated silica supports for catalysis. *Catal. Today* **2001**, *66*, 75–79. [CrossRef]
39. Galarneau, A.; Desplantier, D.; Dutartre, R.; di Renzo, F. Micelle-templated silicates as a test bed for methods of mesopore size evaluation. *Microporous Mesoporous Mater.* **1999**, *27*, 297–308. [CrossRef]